Reentrant Origami-Based Metamaterials with Negative Poisson's Ratio and Bistability

H. Yasuda and J. Yang

Phys. Rev. Lett. **114**, 185502 — Published 5 May 2015

DOI: 10.1103/PhysRevLett.114.185502

Re-entrant origami-based metamaterials with negative Poisson's ratio and bistability

H. Yasuda[1] and J. Yang*[2]

[1]*Department of Mechanical Engineering, University of Washington, Seattle, WA 98195*
[2]*Department of Aeronautics and Astronautics, University of Washington, Seattle, WA 98195*

(Dated: April 23, 2015)

We investigate the unique mechanical properties of re-entrant 3D origami structures based on the Tachi-Miura Polyhedron (TMP). We explore its potential usage as mechanical metamaterials that exhibit tunable negative Poisson's ratio and structural bistability simultaneously. We show analytically and experimentally that the Poisson's ratio changes from positive to negative and vice versa during its folding motion. In addition, we verify the bistable mechanism of the re-entrant 3D TMP under rigid origami configurations without relying on the buckling motions of planar origami surfaces. This study forms a foundation in designing and constructing TMP-based metamaterials in the form of bellows-like structures for engineering applications.

Origami is defined as the handcrafted art of paper folding. In recent decades, origami has attracted significant interest of mathematicians and engineers, not only because it stimulates intellectual curiosity, but also because it has large potentials for engineering applications. One good example is the usage of origami-patterns for the enhancement of structural bending rigidity for thin-walled cylindrical structures [1]. By leveraging their compactness, origami structures are also employed for space applications, such as space solar sails [2, 3] and deployable solar arrays [4]. It is not surprising that biological systems exhibit origami patterns, e.g., tree leaves [5].

Mechanical metamaterials are another topic of active research in the scientific community nowadays. As a counterpart of electromagnetic metamaterials, mechanical ones are constructed in an ordered pattern of unit-cell elements to achieve unusual mechanical properties [6, 7]. Among them are negative Poisson's ratio and controllable instability of structures. For example, negative Poisson's ratio has been exploited to manipulate wave propagation in re-entrant cellular structures [8]. Previous studies also reported that structural instability can be used to achieve tailored damping characteristics in mechanical metamaterials [10, 29].

In this study, we adopt origami structures as a building block of mechanical metamaterials to achieve simultaneous negative Poisson's effect and structural bistability. Specifically, we employ the Tachi-Miura Polyhedron (TMP), which is a bellows-like 3D origami structure based on Miura-ori cells [11, 12] (Fig. 1). Lateral assembly of Miura-ori cells in the form of 2D Miura-ori sheets has been previously explored for the construction of metamaterials [13]. However, there have been limited efforts to study the cylindrical derivative of Miura-ori in the form of TMP [14]. In contrast to 2D origami structures such as Miura-ori sheets and waterbomb [15], the TMP holds a volume that changes continuously from zero to a certain value, and then it returns to zero again at the ends of the folding motion (see Fig. 1(a)). This implies that we can obtain a very large stroke from its folding motion, which is useful in designing actuators and impact absorbers. Also, compared to other origami-based cylindrical structures [16–21], the TMP has a unique feature of rigid foldability. That is, the deformation takes place only along crease lines instead of relying on the elasticity of materials. Therefore, the structure

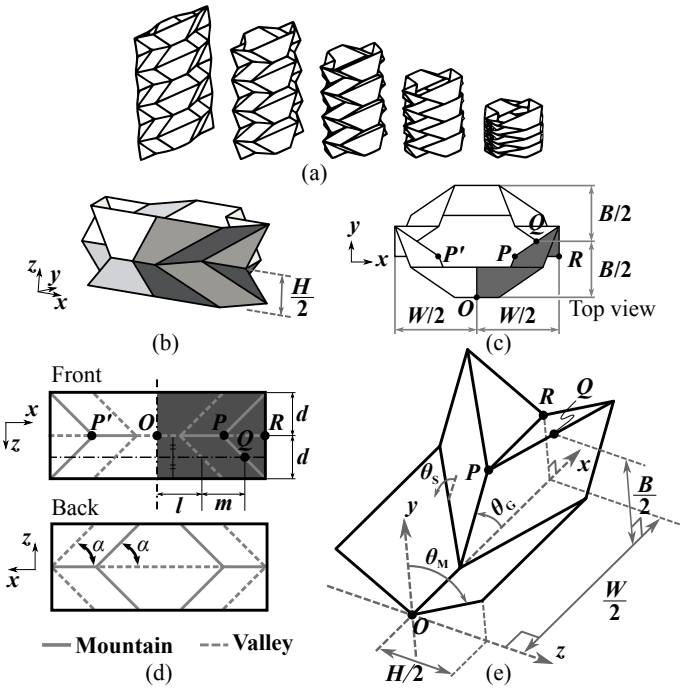

FIG. 1: (a) Folding motion of Tachi-Miura Polyhedron (TMP). (b) Folded TMP cell. (c) Top view of TMP. (d) Flat front and rear sheets of TMP with the crease pattern consisting of mountain and valley folds. (e) Folded configuration of the front sheet corresponding to the shaded areas in (c) and (d).

can consist of only rigid panels and hinges without incurring bending of planar origami surfaces.

In this Letter, we first examine the kinematics of the TMP to show the tunable characteristics of its Poisson's ratio. We verify analytically and experimentally the auxetic effect of volumetric 3D TMP prototypes in bilateral directions, which is an improvement over the conventional 2D origami structures with a single-directional negative Poisson's effect [13, 22, 23]. Second, we investigate the force-displacement relationship of the TMP structure to show that it exhibits bistable nature under the re-entrant configurations. While previous studies investigated structural stability in other types of origami-structures [15, 24–26], bistable – yet foldable – 3D origami

structures without introducing defects have not been reported yet. Lastly, a cellular structure consisting of the TMP cells is explored to form origami-based metamaterials with a view toward potential engineering applications.

We begin with characterizing the geometry of the TMP. Figures 1(b) and (c) show the folded TMP cell in slanted and top views, respectively. This unit cell consists of two flat sheets, whose geometry can be characterized by length parameters (l, m, d) and an inner angle of parallelogram (α) (Fig. 1(d)). The point Q is defined by the two crossing edges of the front and rear surfaces as shown in Fig. 1(c), which passes through the quarter line of the sheets (dash-dot line in Fig. 1(d)). Accordingly, the half breadth ($B/2$) of the TMP cell corresponds to the distance between points O and Q along the y-axis, and the half width ($W/2$) is the distance between points O and R along the x-axis (Figs. 1(c)). The half height ($H/2$) of the TMP cell is also illustrated in Fig. 1(b). Note that the TMP cell exhibits a re-entrant shape when the given geometrical angle α is above 45°.

To calculate W, B, and H under various folding configurations, we consider a quarter model of the TMP (Fig. 1(e)), which corresponds to the dark colored area in Figs. 1(b)-(d). Here, the folding angles, θ_M and θ_S, are functions of α (determined by the given geometry) and θ_G (varies by the degree of folding). The mathematical expressions for these folding angles are described in supplemental document. It should be noted that while $\theta_M \in [0, 90^\circ]$ and $\theta_S \in [0, 90^\circ]$, the range of α is limited to satisfy $2l - d\cot\alpha + 2m\cos 2\alpha > 0$. This is to avoid the collision between points P and P' during folding. Accordingly, $\theta_G \in [0, 2\alpha]$. Based on the geometry described in Fig. 1, W, B, and H are obtained as follows:

$$\begin{aligned} B &= 2m\sin\theta_G + d\cos\theta_M \\ W &= 2l + \frac{d}{\tan\alpha} + 2m\cos\theta_G \\ H &= 2d\sin\theta_M. \end{aligned} \tag{1}$$

We investigate the Poisson's ratios of the TMP by defining them as

$$\nu_{HB} = -\frac{(dB/B\,)}{(dH/H\,)} \quad \text{and} \quad \nu_{HW} = -\frac{(dW/W\,)}{(dH/H\,)}. \tag{2}$$

Differentiating Eq. (1) with respect to the folding angles and plugging them into Eq. (2), we obtain the Poisson's ratios as follows:

$$\begin{aligned} \nu_{HB} &= \frac{4m\tan\alpha\cos\theta_G\cos^2(\theta_G/2) + d}{2m\sin\theta_G + d\cos\theta_M}\sin\theta_M\tan\theta_M \\ \nu_{HW} &= -\frac{4m\tan\alpha\sin\theta_G\cos^2(\theta_G/2)}{2l + (d/\tan\alpha) + 2m\cos\theta_G}\sin\theta_M\tan\theta_M. \end{aligned} \tag{3}$$

To verify this analytical expression, we fabricate three prototypes of the TMP ($\alpha = 30^\circ$, 45°, and 75°) by using paper (See supplemental document for details). The number of Miura-ori layers used in each configuration is $N = 7$, and the characteristic lengths of the prototypes are identical ($l = m = 50$ mm and $d = 30$ mm). We conduct three measurements of B and W at each H, as we gradually change the folding angle. We compare the measured Poisson's ratios with the analytical results from Eq. (3).

Fig. 2 shows the Poisson's ratios as a function of a folding ratio defined as $(90^\circ - \theta_M)/90^\circ$. The Poisson's ratio ν_{HW} in the case of $\alpha = 45^\circ$, 30°, and 70° are plotted in Fig. 2(a), while the insets show the folded configurations under $\alpha = 70^\circ$. We find ν_{HW} is always negative regardless of the folding ratio and α. On the other hand, the Poisson's ratio ν_{HB} related to width B is positive in the initial folding stage, and it approaches zero. It is notable that in the re-entrant case (e.g., $\alpha = 70^\circ$), ν_{HB} becomes negative as shown in Fig. 2(b). As seen in the inset, we evidently observe that B increases and then decreases as the folding ratio of the re-entrant TMP increases. We find excellent agreement between the experimental and analytical results. The areal change of the TMP is also measured and compared with the analytical predictions in the supplemental document.

The analytical contour plot of ν_{HB} as a function of continuous α and the folding ratio is shown in Fig. 2(c). If α is above approximately 55°, ν_{HB} becomes negative during the folding motion. Fig. 2(d) also shows the contour plot of ν_{HB} but $d = 60$ mm. By choosing a certain α angle (e.g. $\alpha = 70^\circ$ as shown in the inset of Fig. 2(d)), we observe ν_{HB} changes from positive to negative in the initial folding stage, and then it becomes positive again around 62 %. The sign of ν_{HB} changes multiple times in one folding motion. This is a unique feature of the TMP compared to the conventional 2D Miura-ori, in which negative Poisson's effect has been reported, but multiple sign flips of the Poisson's ratio has not been discovered [13, 22, 23]. Solving $dB = 0$, we obtain the analytical expression for the transition between positive and negative ν_{HB}:

$$\cos^2\theta_M = \frac{2m\tan\alpha - d \pm 2\sqrt{m\tan\alpha\,(m\tan\alpha - 2d)}}{d\tan^2\alpha}. \tag{4}$$

This boundary is plotted in a dashed curve in Fig. 2(c,d).

Now we investigate force and folding ratio relationship to validate the bistable nature of the TMP. We model the TMP by rigid plates connected by torsional spring along the crease lines (see supplemental document for details). We consider the folding behavior of the TMP under a uniaxial force (F) in the z-direction. By applying virtual displacement (δu) to the TMP and using the principle of virtual work, we obtain the following equation:

$$F\delta u = 2n_M M_M \delta\theta_M + 2n_S M_S \delta\theta_S, \tag{5}$$

where $n_M = 8(N-1)$ and $n_S = 8N$ are the number of horizontal and inclined crease lines related to θ_M and θ_S respectively, and M_M (M_S) is the bending moment along horizontal (inclined) crease lines. Let the torsional spring constant be k_θ, assuming that the torsion spring is linear and identical throughout all crease lines. Mathematically, this can be

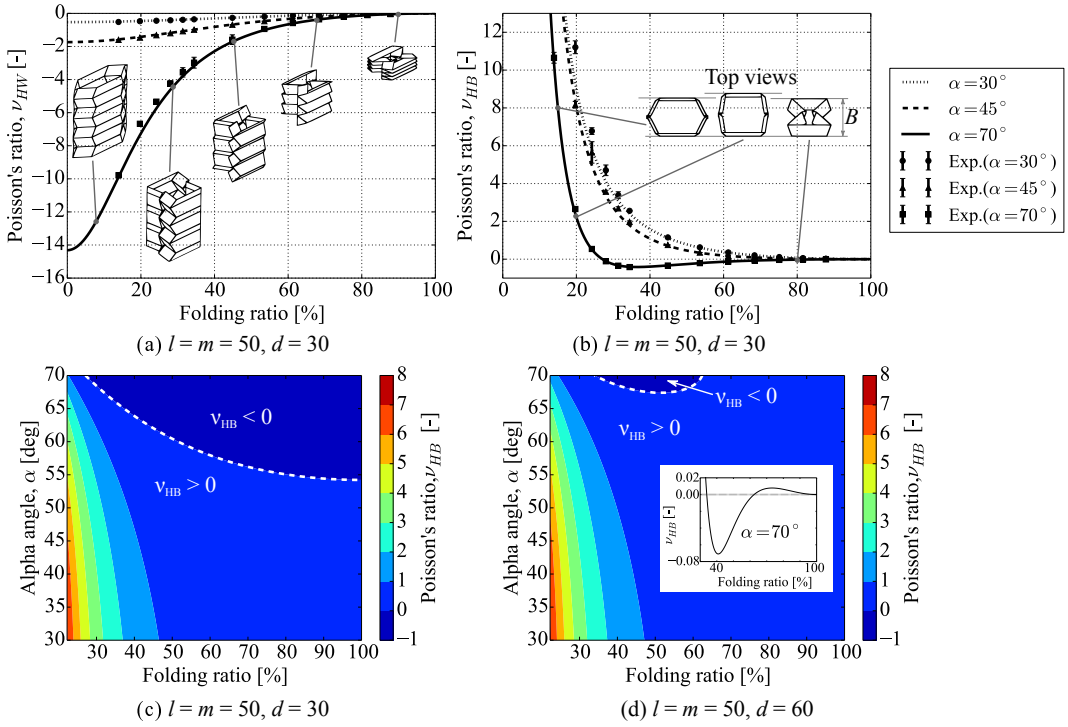

FIG. 2: Poisson's ratio change of TMP. (a) ν_{HW} and (b) ν_{HB} as a function of the folding ratio. Insets show folded configurations of re-entrant TMP under $\alpha = 70°$ and $l = m = 50, d = 30$ mm. Errorbars indicate standard deviations. Contour plot of ν_{HB} as a function of α and the folding ratio if (c) $d = 30$ and (d) $d = 60$. The white dashed line indicates the boundary between positive and negative ν_{HB}.

expressed as $M = 2k_\theta\left(\theta - \theta^{(0)}\right)$ where $\theta^{(0)}$ is the initial folding angle (i.e., natural angle with no potential energy). Based on the geometry of the TMP and Eq. (5), the compressive force can be expressed as (see supplemental document for details):

$$\frac{F}{(k_\theta/d\,)} = -\frac{32}{\cos\theta_M}\left\{\frac{N-1}{N}\left(\theta_M - \theta_M^{(0)}\right) + \left(\theta_S - \theta_S^{(0)}\right)\frac{\cos^3\frac{\theta_G}{2}\sin\theta_M}{\cos\alpha\sin\theta_S}\right\}. \tag{6}$$

Note that we use a normalized force to remove the effect of spring coefficient and the dimension of the TMP.

Figure 3 shows the force-folding ratio relationship of the TMP under different initial conditions. When the natural folding angle $\theta_M^{(0)}$ is $45°$ and the number of layers N is 7, the normalized force increases monotonically regardless of α values as shown in Fig. 3(a). However, in the case of $\theta_M^{(0)} = 80°$ (i.e., a more upward initial posture than $\theta_M^{(0)} = 45°$), we observe the TMP with $\alpha = 70°$ exhibits a local minimum point in the force-folding relationship (see the solid curve in Fig. 3(b)). This indicates that the re-entrant structure under $\theta_M^{(0)} = 80°$ and $\alpha = 70°$ has two stable configurations: one is the initial state (the folding ratio of 11%) and the other is a state in the middle of the folding motion (folding ratio of about 67%). At certain geometrical and folding configurations, the 3D TMP structure can exhibit two or even three different equilibrium states under the same normalized force (see supplemental document for an example of $F/(k_\theta/d) = 45$). We also note that this can incur an interesting phenomenon, such as negative stiffness, snap-through and hysteresis effects, which can be exploited for the purpose of energy absorption and impact mitigation.

We now investigate numerically the local minimum points under various combinations of α and $\theta_M^{(0)}$ values (Fig. 3(c)). We observe that the bistability arises when the TMP exhibits re-entrant shapes and appropriate initial folding angles are applied (minimal $\theta_M^{(0)}$ is $73°$ given the geometry), implying that by changing $\theta_M^{(0)}$, one can manipulate the stability of the TMP.

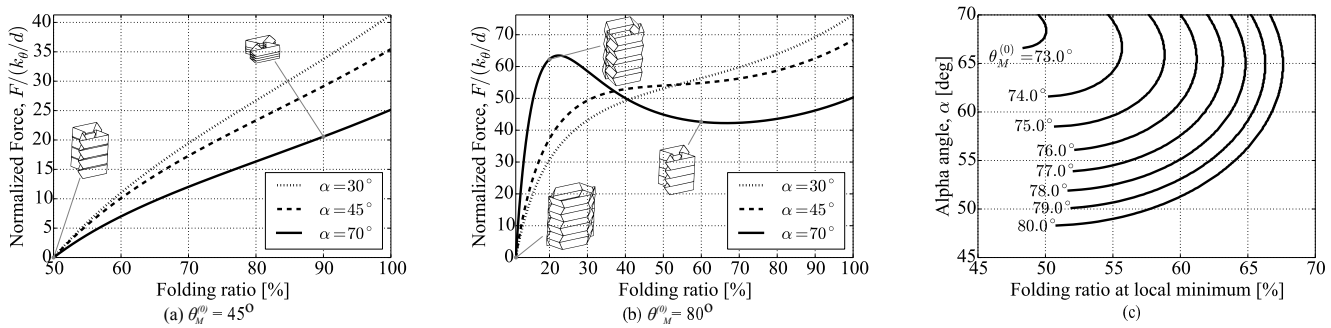

FIG. 3: Force-folding ratio relationship. The number of layers N is 7, and initial folding angle is (a) $\theta_M^{(0)} = 45^\circ$ and (b) $\theta_M^{(0)} = 80^\circ$. Illustrations indicate the folded shape of the TMP with $\alpha = 70^\circ$. (c) Folding ratio at local minimum point under different initial angles $\theta_M^{(0)}$.

It should be noted that the bistability in this TMP structure is achieved solely by its kinematics, without relying on material properties or deformation of the facets. While previous studies discovered simultaneous foldability and bistability in the setting of 2D origami cells [26], a 3D version of such architectures has been unexplored. Thus, the TMP can serve as a prototypical 3D origami structure, which exhibits foldability and bistability at the same time. The bistable characteristic can provide self-locking mechanisms, so that the structure can cease its folding motion and maintain a certain folded configuration stably.

Lastly, we explore the design of a cellular structure consisting of multiple TMP cells (Fig. 4). Similar to its unit cell, this TMP cellular structure transforms from a 2D state to another 2D configuration, while filling 3D space in the transition stage. Therefore, by taking advantage of the unique kinematics of the TMP unit cell discussed above, we can design a new type of 3D structures which exhibit tunable Poisson's ratio and structural bistability. Figure 4(a) shows the TMP cellular structure with $\alpha = 30^\circ$, where we observe the structure stretches in the y-direction while being contracted in the x-direction monotonically (i.e., positive ν_{HB} and negative ν_{HW}). If $\alpha = 70^\circ$, it expands in the y-direction at first behaving similar to the previous case, but past a certain threshold, it starts to shrink in all directions as shown in Fig. 4(b) due to the negative Poisson's ratios in bilateral directions. These TMP cellular structures are also one degree-of-freedom system. Therefore all TMP cells fold and unfold simultaneously by manipulating one parameter, folding angle θ_M in this study.

In conclusion, we investigated unique kinematics of origami-based 3D structures based on the Tachi-Miura Polyhedron (TMP). We found that the Poisson's ratio of the re-entrant TMP can be tuned to exhibit negative values in bilateral directions under the strains along the stacking direction. Also, the re-entrant TMP can exhibit bistable characteristics in contrast to normal TMP configurations. The findings in this study can form a foundation in designing and constructing a new type of mechanical metamaterials, which feature controllable auxeticity and structural stability. These 3D cellular structures offer an enhanced degree of freedom in structural responses, showing great potentials for various engineering applications such as space structures and impact absorbers.

Acknowledgements. We thank Dr. Richard Wiebe for his helpful input. We acknowledge the support of NSF (CMMI-1414748) and ONR (N000141410388).

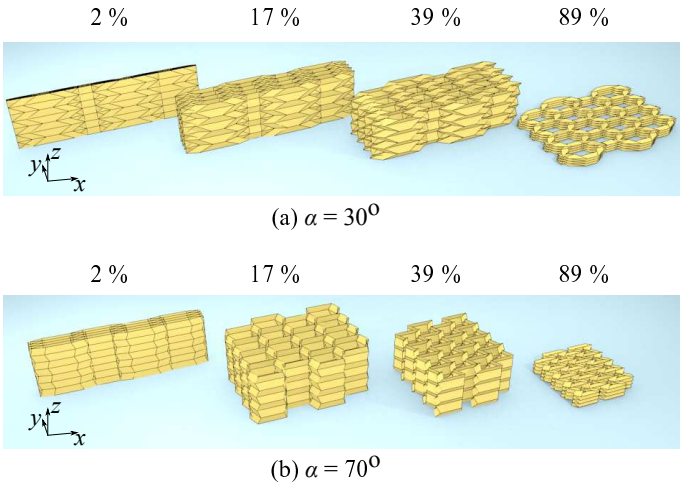

FIG. 4: Folding motions of TMP cellular structures. The numbers show folding ratios, and $l = m = 50$ mm, $d = 30$ mm. (a) $\alpha = 30^\circ$. (b) $\alpha = 70^\circ$.

[1] K. Miura, in *Proceedings of IASS Symposium on Folded Plates and Prismatic Structures*, (1970).

[2] O. Mori, H. Sawada, R. Funase, M. Morimoto, T. Endo, T. Yamamoto, Y. Tsuda, Y. Kawakatsu, J. Kawaguchi, and I. D. T. and S. W. Group, in *Proceedings of the 27th International Symposium on Space Technology and Science*, 2009o407v, (2009).

[3] Y. Tsuda, O. Mori, R. Funase, H. Sawada, T. Yamamoto, T. Saiki, T. Endo, and J. Kawaguchi, Acta Astronaut., **69**, 833840 (2011).

[4] S. A. Zirbel, R. J. Lang, M. W. Thomson, D. A. Sigel, P. E. Walkemeyer, B. P. Trease, S. P. Magleby, and L. L. Howell, J.

Mech. Des., **135**, (2013).
[5] H. Kobayashi, B. Kresling, and J. F. V. Vincent, Proc. R. Soc. Lond. B, **265**, 147154 (1998).
[6] Z. Liu, X. Zhang, W. Mao, Y. Zhu, Z. Yang, C. Chan, P. Sheng, Science, **289**, 5485 (2000).
[7] M. Maldovan, Nature, **503**, 209217 (2013).
[8] M. Ruzzene, F. Scarpa, F. Soranna, Smart Mater. Struct., **12**, 363 (2003).
[9] L. Dong, R. Lakes, Smart Mater. Struct., **21**, 075026 (2012).
[10] P. Wang, F. Casadei, S. Shan, J. Weaver, K. Bertoldi, Phys. Rev. Lett. **113**, 014301 (2014).
[11] K. Miura and T. Tachi, in *Symmetry Art Sci. 2010/1-4, Spec. Issues Festival-Congress, ISIS-Symmetry (International Soc. Interdiscip. Study Symmetry) Gmuend*, Austria, 204-213 (2010).
[12] T. Tachi, in *Symp. of the Int. Association for Shell and Spatial Structures (50th. 2009. Valencia). Evolution and Trends in Design, Analysis and Construction of Shell and Spatial Structures: Proceedings (eds A Domingo, C Lazaro)* 2295-2305 (2010).
[13] M. Schenk and S. D. Guest, Proc. Natl. Acad. Sci. USA. **110**, 32763281 (2013).
[14] H. Yasuda, T. Yein, T. Tachi, K. Miura, and M. Taya, Proc. R. Soc. A, **469**, 20130351 (2013).
[15] B. H. Hanna, J. M. Lund, R. J. Lang, S. P. Magleby, and L. L. Howell, Smart Mater. Struct., **23**, 094009 (2014).
[16] S. D. Guest and S. Pellegrino, J. Appl. Mech., **61**, 773777 (1994).
[17] G. W. Hunt and I. Ario, Int. J. Non. Linear. Mech., **40**, 833843 (2005).
[18] Z. You and K. Kuribayashi, in *Origami 4. Fourth International Meeting of Origami Science, Mathematics and Education*, Pasadena, U.S.A., September 2006, edited by R. J. Lang, 117127, A K Peters (2009).
[19] J. Song, Y. Chen, and G. Lu, Thin-Walled Struct., **54**, 6571 (2012).
[20] J. Ma and Z. You, J. Appl. Mech., **81**, 011003 (2014).
[21] S. Ishida, T. Nojima, and I. Hagiwara, J. Mech. Des., **136**, 091007 (2014).
[22] Z. Y. Wei, Z. V. Guo, L. Dudte, H. Y. Liang, and L. Mahadevan, Phys. Rev. Lett. **110**, 215501 (2013).
[23] C. Lv, D. Krishnaraju, G. Konjevod, H. Yu, and H. Jiang, Sci. Rep. **4**, 5979 (2014).
[24] J. L. Silverberg, A. A. Evans, L. McLeod, R. C. Hayward, T. Hull, C. D. Santangelo, and I. Cohen, Science, **345**, 647 (2014).
[25] K. Saito, A. Tsukahara, and Y. Okabe, J. Mech. Des., **137**, 021402 (2015).
[26] S. Waitukaitis, R. Menaut, B. G. Chen, and M. van Hecke, Phys. Rev. Lett. **114**, 055503 (2015).
[27] See Supplemental Material [url], which includes Refs. [28-29].
[28] W. S. Rasband, ImageJ, U. S. National Institutes of Health, Bethesda, Maryland, USA, 1997-2014. (`http://imagej.nih.gov/ij/`)
[29] L. Dong and R. S. Lakes, Smart Mater. Struct. **21**, 075026 (2012).